Enhancement of heat transfer through the incorporation of copper metal wool in latent heat thermal energy storage systems

Renewable Energy 231 (2024) 120888

Contents lists available at ScienceDirect

Renewable Energy

journal homepage: www.elsevier.com/locate/renene

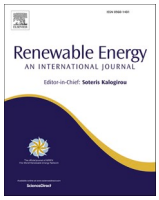

Enhancement of heat transfer through the incorporation of copper metal wool in latent heat thermal energy storage systems

Alessandro Ribezzo [a], Matteo Morciano [a], Gabriel Zsembinszki [b], Sara Risco Amigó [b], Saranprabhu Mani Kala [b], Emiliano Borri [b], Luca Bergamasco [a], Matteo Fasano [a], Eliodoro Chiavazzo [b], Cristina Prieto [c], Luisa F. Cabeza [a,*]

[a] Department of Energy, Politecnico di Torino, Corso Duca degli Abruzzi 24, 10129, Torino, Italy
[b] GREiA Research Group, University of Lleida, Pere de Cabrera s/n, 25001, Lleida, Spain
[c] University of Seville, Department of Energy Engineering, Camino de los Descubrimientos s/n, 41092, Seville, Spain

ARTICLE INFO

Keywords:
Thermal energy storage
Phase change materials
Experimental study
Heat transfer enhancement
Metal wool

ABSTRACT

The design of thermal energy storage (TES) tank is the key part that can limit charging and discharging process. Most research findings highlight that the use of fins augments the heat transfer rate. This work experimentally investigates the use of aligned copper wools as fillers to enhance the thermal performance of a lab-scale shell-and-tube TES tank filled with phase change material (PCM). Two copper wools with different fibre thicknesses were chosen and discretely laid around the TES tank tubes in two design patterns. Accordingly, five shell-and-tube TES tank configurations were obtained, including the reference, for performance evaluation. The TES tank was loaded with n-octadecane as PCM for all the cases studied. The results showed up to a 16 % reduction in melting time with the inclusion of copper wool. The TES tank significantly increased the mean power during charging (53 %) and discharging (205 %). The addition of metal wool into the TES tank enables the PCM to release the heat at a constant temperature during the entire phase transition process. And the overall efficiency of the TES tank was found to get improved. Therefore, a copper wool integrated TES tank would be a beneficial addition to thermal energy storage systems.

1. Introduction

The world energy demand is increasing exponentially due to urbanization and the advancement of industrial sectors. Fossil fuels were found to be significant energy sources to address the growing energy needs. However, there is an outbreak of CO_2 emissions due to the extensive usage of fossil fuels, which turns out to be a significant threat heading to climatic change, ozone layer depletion, and several other problems [1]. These issues can be alleviated through the productive utilization of renewable energy sources [2]. However, renewables suffer from its intermitting behaviour, which causes a mismatch between the power production and energy demand.

Thermal energy storage (TES) is a technology able to store energy in the form of heat with the benefit of retrieving the stored energy according to demand [3]. The TES systems are categorized as sensible heat TES systems, latent heat TES systems, and chemical storage and sorption (also known as thermochemical) TES systems. Latent heat TES system may use phase change material (PCM) as a storage medium due to its high energy storage capacity during phase transition [4,5]. The essential parts of a latent heat TES systems are the thermal energy source (i.e., solar energy, waste heat), working fluid, phase change material, the TES tank, and the energy sink (i.e., heating system, power cycle). By understanding the TES system operation, one could figure out the significance of these components. The inlet thermal energy will be pumped by the working fluid in a real-time TES system. Once the fluid flows through the energy source, it begins to heat up and then arrives in the TES tank, which holds the PCM. At this point, the PCM and working fluid exchange thermal energy, and therefore the TES tank is filled. When needed, the stored energy can be obtained by pumping a working fluid across the TES tank bringing the thermal energy to the final application.

Although the use of PCM in TES systems has substantial benefits, it also suffers from significant problems [6]. The most common issue associated with the use of PCMs is their low thermal conductivity, which influences the TES system thermal performance resulting in time

* Corresponding author.
E-mail address: luisaf.cabeza@udl.cat (L.F. Cabeza).

https://doi.org/10.1016/j.renene.2024.120888
Received 2 February 2024; Received in revised form 30 May 2024; Accepted 27 June 2024
Available online 27 June 2024

demanding charging and discharging processes [7]. Considerable research was carried out to improve the TES system thermal performance. The most studied approaches are categorized as (i) enhancing the thermophysical properties of the PCM employed and (ii) modifying the design of the TES tank. The techniques to enhance the thermophysical properties of the PCM include the addition of nanoparticles and micro or macro encapsulation of phase change materials [8–12]. At the same time, including metal foams, metal wool, and fins in a heat exchanger unit was also found to be an effective strategy to promote the thermal performance of the TES system by enhancing heat transfer via conduction [13–15].

Belazreg et al. [16] numerically studied the thermal performance of the shell-and-tube TES tank by incorporating Y-shaped longitudinal fins of 4 mm to the tube side of the TES tank. The authors developed three different cases of TES tanks: Case (i) containing only PCM; Case (ii) including two Y-shaped fins; Case (iii) including four Y-shaped fins. A significant reduction in the melting time was observed for the TES tank built with four Y-shaped fins. The authors reported that the increased number of fins reduced the thermal resistance within the TES tank, thus enhancing the heat transfer rate. Surya et al. [17] developed PCM-loaded stainless steel balls with rod-shaped internal fins to improve the TES thermal performance. The authors observed a 47.37 % reduction in the time required for charging the PCM for the fins-incorporated stainless-steel ball. Xu et al. [18] proposed an intelligent memory fin technique to promote the charging and discharging performance of the PCM. The titanium-nickel alloy memory fin measures 55 mm × 20 mm X 1 mm. The memory fin incorporated tends to bend when exposed to elevated temperatures. The study reported a 28.6 % reduction in melting time using a memory fin instead of a standard fin. The authors reported that during the mid-stage of the charging cycle, the fin bends and squeezes the liquid PCM underneath to make it flow to the top surface, promoting natural convection effects. The enhanced natural convection effects reduce the time required for melting the PCM. Al-Abidi et al. [13] numerically investigated the impact of integrating internal and external fins into a triplex tube heat exchanger-based TES tank. The authors developed different cases of TES tanks by varying the PCM employed, Stefan number, fin numbers, fin length, and fin thickness. The results showed that all the parameters except fin thickness have a reasonable influence on the thermal performance of the TES tank.

Prasanth et al. [19] developed latent heat thermal energy storage systems integrated with Cu foam, Cu wire foam and Al wire foam, aiming to improve the thermal conductivity of the PCM (paraffin wax). The authors reported an 18.9 % and 15.5 % reduction in melting time for the Cu foam-incorporated paraffin wax and Al wire foam-incorporated paraffin wax latent heat thermal energy storage system, respectively. Morciano et al. [20] incorporated a 3D-printed cartesian lattice metal structure into a TES system to encompass the PCM. The lattice metal structure was made up of aluminium alloy AlSi10Mg. The authors observed a remarkable heat transfer rate within the TES tank during the charging and discharging cycles (714 W/kg and 1310 W/kg, respectively).

Metal wool appear to be a good solution for improving the effective thermal conductivity of PCMs as well as the thermal performance of TES systems. Metal wool offers more beneficial characteristics compared to present techniques for improving the thermal transfer properties of the TES tank. Metal wool has a high porosity structure and can accommodate the same amount of PCM as a conventional shell and tube TES tank. Metal wool provides a long heat conduction path, facilitating heat transfer within the phase transition material. It is a low-cost enhancer that can be integrated into any system, making it suitable for a wide range of applications.

Favache et al. [21] employed aluminium metal wool to improve the thermal transfer characteristics of a paraffin-loaded TES system. The author developed three distinct configurations of a metal wool-incorporated TES tank by altering the mass percentage of metal wool relative to PCM mass, with the maximum metal wool added being 18 %. The author reported that the effective thermal conductivity of the PCM increased in the solid phase rather than the liquid phase because the metal wool acts as a barrier, reducing the movement of natural convection effects occurring in the liquid phase. The author concluded that the inclusion of metal wool has a considerable effect on solidification time but not on the melting time. Prieto et al. [22] employed metal wool to improve heat transfer in the sodium nitrate-loaded TES system. The author used stainless steel metal wool in 16 layers in diverse directions, but always perpendicular to the HTF tubes. The author claimed a 300 % increase in solid-state thermal conductivity of NaNO3 incorporated with metal wool. Gasia et al. [23] experimentally investigated the effect of adding fins and metal wool to the TES tank. The authors reported that the TES tank that contains fins attained the highest heat transfer rate compared to the other configurations.

Based on the literature review, it is evident that increasing the heat transfer surface area certainly enhances the thermal performance of the TES system [24]. Most of the research studies employ fins compared to other techniques [25–27]. While, in most studies, the performance of the TES system was numerically investigated [28,29], in the case of metal wool, the available works in the literature are still limited [30]. No research papers were identified that discuss employing copper metal wool as an option to increase the effective thermal conductivity of PCM tanks. To the authors knowledge, there are also no such studies that consider the thickness of the metal wool and the design pattern of metal wool laid in TES tanks.

This study stands out for incorporating aligned (i.e. fibre oriented in a one particular direction) copper wool as a heat transfer enhancer for the TES tank. The most important benefit of adding metal wool is that the thermal performance of the TES tank can be improved without significantly affecting the energy storage density of the PCM. The thermal performance improvement is obtained as the increase in effective heat transfer surface area between the heat transfer fluid (HTF) and the PCM. Importantly, it is a technology that can be implemented to an existing TES tank, without the requirement of a complete redesign of the system. Copper wools of two dissimilar thicknesses (coarse and fine) were utilized for this study and incorporated in two different configurations. Accordingly, four cases of TES tank configurations have been developed, plus the baseline configuration that contains no metal wool. Charging and discharging cycles were experimentally tested for all the cases.

2. Materials and methods

2.1. Materials

In this study, N-octadecane ($CH_3(CH_2)_{16}CH_3$)) was chosen as PCM for the TES tank, procured from Alfa Aesar, Germany. Copper wools of two different thicknesses procured from STAX, Germany, were utilized as heat transfer enhancers. Table 1 details the specific properties of the n-octadecane and the copper wool. Fig. 1 shows the optical images of the copper wools. The TES tank used for this study resembles a shell-and-tube heat exchanger-based design with a volumetric capacity of 3 L.

Table 1
Specific properties of n-octadecane and copper wool (*Information provided by the manufacturer*).

Description	Filler (metal wool)	Phase change material
Material	Copper	n-octadecane
Purity	99 %	90 %
Density	8.9 g/cm^3	0.782 g/cm^3
Thermal conductivity	383 W/m·K (single fiber)	0.153 W/m·K [31]
Thickness	Coarse: 120 μm Fine: 60 μm	n.a.
Melting point	n.a.	28 °C
Latent heat	n.a.	243.5 J/g [32]

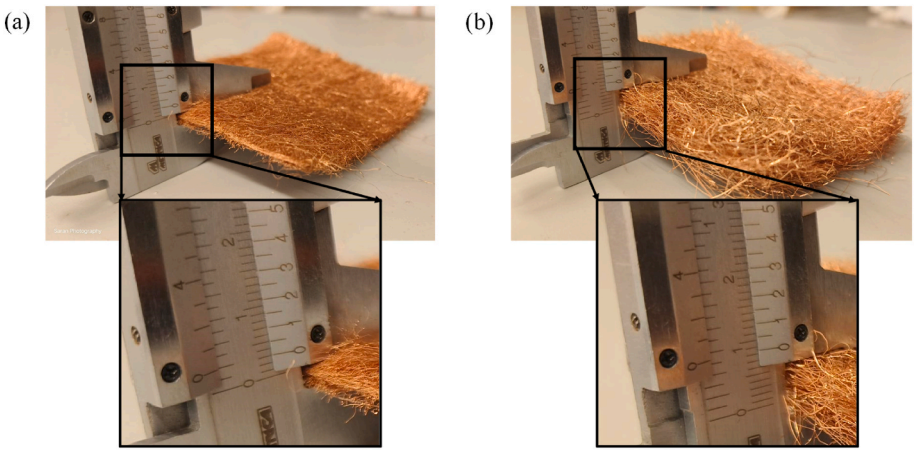

Fig. 1. Images of (a) fine and (b) coarse copper wool.

2.2. Analytical methods

The heat flow vs. temperature data for the PCM (n-octadecane) was acquired using differential scanning calorimeter (DSC) equipment (DSC 3+, Mettler Toledo). The aluminium crucible was loaded with the determined sample mass to be tested. The instrument analyses the sample under a nitrogen atmosphere. The heat flow curve was recorded within the temperature range from 15 °C to 35 °C to cover the phase transition interval of the n-octadecane. The measurements were repeated three times at 1 K/min heating rate for uncertainty analysis.

2.3. Experimental setup

The charging and discharging characteristics of the tailor-made TES tank were acquired using the *in-house* experimental setup. The setup includes a refrigeration unit, a buffer tank with two in-built heaters, water pumps, a flow meter, and the TES tank of interest (Fig. 2). 12.7 mm diameter sized copper pipes interconnect the components hydraulically. Polyurethane envelope insulates the copper pipes to reduce the heat loss to the surroundings. The TES tank was loaded with the same mass of n-octadecane (2.1 kg) regardless of the configurations. Generally, the heat transfer fluid (HTF) selection relies on the working temperature range. In this study, the operating temperature range stretches between 15 ± 1 °C to 45 ± 1 °C; subsequently, water was chosen as an appropriate HTF.

The HTF in the buffer tank can be taken to high temperatures using the built-in heaters and to low temperatures using the condensing unit. A buffer tank with a capacity of 200 L was selected to deliver the HTF at a nearly constant temperature to the TES tank. The water pump drives the HTF between the buffer tank and the TES tank at a constant flow rate. PT-100 temperature sensors with an accuracy of ±0.3 °C were utilized to acquire temperature measurements: i) of the PCM and ii) of the HTF at the inlet and outlet sections of the TES tank. The temperature measurements of all the temperature sensors were acquired every 10 s by the data acquisition system. Three temperature sensors were mounted at different spots in the buffer tank to measure its temperature, and the average of their measurements was used to figure out the buffer tank temperature. Nine temperature sensors were utilized in the experimental setup to measure the temperature of the confined PCM in the TES tank. The first four temperature sensors (T1 to T4) were placed in the anterior region of the TES tank, evenly spaced apart, and the next four temperature sensors (T5 to T8) at the tank's posterior position. However, the positioning of each temperature sensor was done to provide for accurate measurement of the PCM's temperature at various tank levels and in close proximity to the HTF tubes. Besides these, another temperature sensor (T9) was placed in the tank posterior area, but it

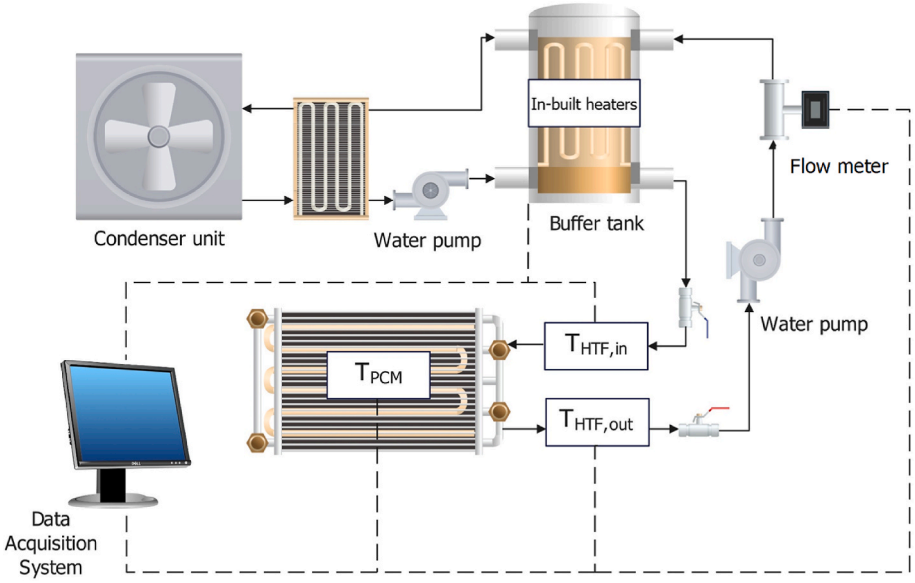

Fig. 2. Schematic representation of the experimental setup.

measures the temperature of the PCM deep inside the tank. This temperature sensor is deliberately placed to measure the temperature of the PCM, which has a greater temperature differential with the HTF tubes and will undergo phase transition later. Measuring the temperature at this position confirms that the phase change has occurred across all cross-sections of the TES tank. An application to control the components of the setup was developed utilizing InduSoft Web Studio. Table 2 provides the details on the main parts of the experimental setup. The schematic representation of the TES tank and the position of temperature sensors are shown in Fig. 3.

2.4. Methodology

2.4.1. tank design

Five shell-and-tube TES tank configurations were developed with n-octadecane as the PCM and copper wool as fillers. The baseline design only contains the PCM, deliberately designed to be used as a reference for comparing the performance of the different configurations with the copper wool embodied in the TES tank. The other four cases differ in the thickness of the copper wool (fine and coarse fibres) and the design pattern by which the copper wool was embodied in the TES tank. It entails that every configuration has a different packaging factor. Where, the packaging factor is defined as the metal wool mass divided by the TES tank volume. The copper wool was laid perpendicular to the HTF tubes for all four cases to enhance the heat transfer in the radial direction. Fig. 4 shows the schematic representation of the five configurations, and their detailed specifications are reported in Table 3. Fig. 5 shows the images of the TES tank and the copper wool incorporated TES tank. To avoid heat losses, the TES tank was covered with insulation (polystyrene, ~80 mm thick) on all sides. Additionally, in order to keep the ambient temperature identical across all of the tests, the experiments were carried out at the same time on subsequent days in a closed lab atmosphere.

2.4.2. Charging and discharging cycles

Before each charging cycle, the PCM temperature was brought down to 15 ± 1 °C. This was achieved using the refrigeration unit that cooled the buffer tank, and the cold water was pumped to the TES tank to cool the PCM Then, the buffer tank was heated by the built-in heaters to reach 46 ± 1 °C. Once the buffer tank reached the set temperature, the hot water was pumped at 3 L/min through the tube side of the TES tank to charge (heat) the PCM. In this process, the PCM temperature increased from 15 ± 1 °C to 45 ± 1 °C and the PCM underwent a phase transition from solid to liquid phase.

During the discharging cycle, the PCM was cooled from 45 ± 1 °C to 15 ± 1 °C. All discharging cycles were carried out immediately after a charging cycle, to take advantage of the fact that the PCM temperature was around 45 ± 1 °C at the end of a charging cycle. Accordingly, the buffer tank was cooled down to 14 ± 1 °C using the refrigeration unit before starting the discharging cycle. Once the buffer tank reached the prerequisite temperature, the cold water was pumped at 3L/min through the tube side of the TES tank to discharge (cool) the PCM. In this process, the PCM temperature decreased from 45 ± 1 °C to 15 ± 1 °C and the PCM underwent a phase transition from liquid to solid phase.

Table 2
Specifications of the custom-built experiment facility.

Description	Manufacturer	Model and specifications
Refrigeration unit	Zanotti uniblock	GCU2030ED01B
In-built heater	n.a.	3 kW
Water pump	Pentax	PM45 0.5 HP
Flow meter	ModMAG	M1000
Temperature sensors	n.a.	Pt-100 1/5 DIN class B Pt-100 class B, IEC 60.751
Data logger	STEP	DL01-CPU
Control program	Indusoft Web studio	Version 8.1

The charging and discharging cycles of all five configurations were repeated three times for uncertainty analysis. The operating conditions of the experimental setup are reported in Table 4.

The mean power of the TES tanks during the charging cycle and discharging were estimated using the following expression.

(a) Charging cycle:

$$P_{ch} = \frac{\sum_{T_{PCM=15\ ^\circ C}}^{T_{PCM=29\ ^\circ C}} \dot{m}_{HTF} C_p \left(T_{HTF,in} - T_{HTF,out}\right) \Delta t}{t_{ch}} \quad (1)$$

(b) Discharging cycle:

$$P_{dis} = \frac{\sum_{T_{PCM=45\ ^\circ C}}^{T_{PCM=23.5\ ^\circ C}} \dot{m}_{HTF} C_p \left(T_{HTF,out} - T_{HTF,in}\right) \Delta t}{t_{dis}} \quad (2)$$

The overall efficiency of the TES configurations was estimated using the following expression:

$$\%\eta = \frac{\frac{\sum_{T_{PCM=45\ ^\circ C}}^{T_{PCM=23.5\ ^\circ C}} \dot{m}_{HTF} C_p \left(T_{HTF,out} - T_{HTF,in}\right) \Delta t}{t_{dis}}}{\frac{\sum_{T_{PCM=15\ ^\circ C}}^{T_{PCM=29\ ^\circ C}} \dot{m}_{HTF} C_p \left(T_{HTF,in} - T_{HTF,out}\right) \Delta t}{t_{ch}}} * 100 \quad (3)$$

where η is the overall efficiency, P_{ch} and P_{dis} are the mean power generated by the TES tanks during the charging and discharging cycle, respectively, $\dot{m}_{HTF}$ and C_p are the mass flow rate and the specific heat capacity of the HTF, $T_{HTF,in}$ and $T_{HTF,out}$ are the inlet and outlet temperatures of the HTF associated with the TES tanks during the successive charging and discharging cycles, T_{PCM} is the temperature of the PCM, Δt is the time step between two successive readings, t_{ch} is defined as the time required for the PCM temperature to rise from 15 °C to 29 °C and t_{dis} is the time required for the PCM temperature to drop from 45 °C to 23.5 °C. The temperature extremities were selected based on the heat flow and temperature curve obtained from the differential scanning calorimeter.

The specific heat capacity of the HTF was estimated using the following formula [33]:

$$C_{p,HTF} = 2.69e^{-9} \cdot T_{HTF}^4 - 6.63e^{-7} \cdot T_{HTF}^3 + 2.69e^{-5} \cdot T_{HTF}^2 - 2.69e^{-3} \cdot T_{HTF} + 4.21 \quad (4)$$

2.5. Uncertainty analysis

Measurement uncertainty is related to the random and systematic errors involved in measurement and depends on both the accuracy and precision of the measuring instrument [34]. Therefore, the randomness error (Type – A) and systemic error (Type – B) were considered to determine the total uncertainty, namely:

$$U = \sqrt{U_A^2 + U_B^2} \quad (5)$$

where U_T is the total uncertainty, U_A is the uncertainty due to randomness of the measurement and U_B is the uncertainty due to systemic error.

The total maximum uncertainty in the measurement of charging time was estimated to be 38.9 s. And 0.3 % was reported as the uncertainty in mass flow rate from the manufacturer and the temperature sensor used for the temperature measurements has an accuracy of ±0.3 °C. However, the specific heat capacity of the HTF was obtained from the expression.

The total uncertainty for the measurement “mean power” was

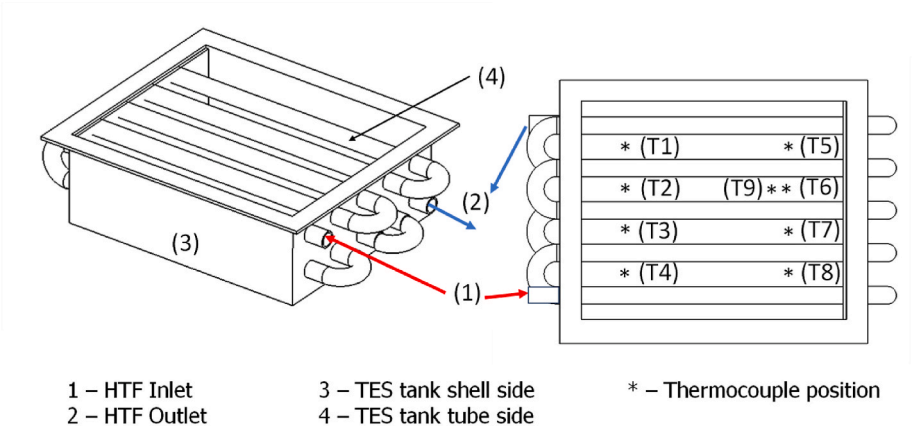

Fig. 3. Schematic representation of the TES tank.

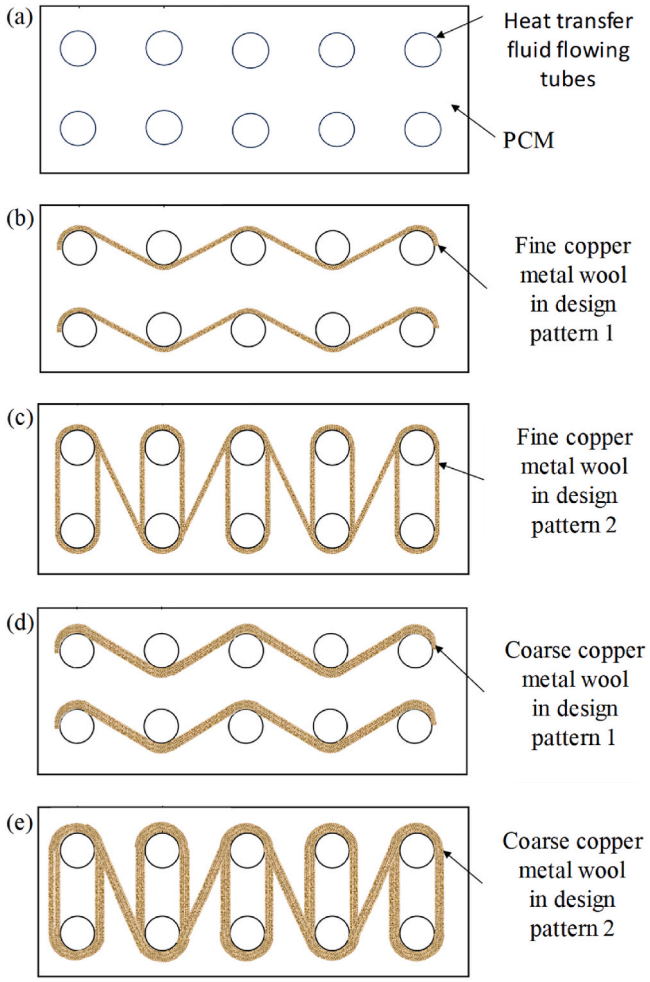

Fig. 4. Schematic representation of copper wool configurations: (a) Baseline – TES tank with only PCM, (b) Case 1 – TES tank with PCM and fine copper wool in design pattern 1, (c) Case 2 – TES tank with PCM and fine copper wool in design pattern 2, (d) Case 3 – TES tank with PCM and coarse copper wool in design pattern 1, and (e) Case 4 – TES tank with PCM and coarse copper wool in design pattern 2.

calculated from the standard error of the mean (Type-A) in the measurement of "mean power" and the uncertainty (Type-B) in the measurement of mass flow rate, two temperatures and two times.

Thus, the total uncertainty of the parameter "mean power" was estimates as follows [34]:

$$U_P = \sqrt{SEM_P^2 + \left(\frac{\partial P}{\partial \dot{m}} \cdot U_{\dot{m}}\right)^2 + 2.\left(\frac{\partial P}{\partial T} \cdot U_T\right)^2 + 2.\left(\frac{\partial P}{\partial t} \cdot U_t\right)^2} \quad (6)$$

where "SEM_P" represents the Type-A uncertainty obtained from the calculation of mean power, "$U_{\dot{m}}$", "U_T" and "U_t" represent the Type-B uncertainty of mass flow rate, temperature and time.

Table 3
Design specifications of the copper wool configurations developed.

Description	Baseline	Case 1	Case 2	Case 3	Case 4
Filler	–	Copper wool	Copper wool	Copper wool	Copper wool
Thickness of metal wool	–	60 μm	60 μm	120 μm	120 μm
Metal wool design pattern	–	Pattern 1	Pattern 2	Pattern 1	Pattern 2
Number of metal wool sheets	–	2 sheets of size 24 × 24 cm	2 sheets of size 24 × 24 cm & 5 sheets of size 24 × 20 cm	2 sheets of size 24 × 24 cm	2 sheets of size 24 × 24 cm & 5 sheets of size 24 × 20 cm
Total length of wool sheets	–	1 sheet of size 48 × 24 cm	1 sheet of size 148 × 24 cm	1 sheet of size 48 × 24 cm	1 sheet of size 148 × 24 cm
Mass of the metal wool	–	245.0 g	437.7 g	369.0 g	841.6 g
Packing factor	–	0.08 g/cm3	0.14 g/cm3	0.12 g/cm3	0.28 g/cm3

3. Results and discussion

3.1. Characterization of the PCM

The data related to the onset, end set, and peak temperatures of the n-octadecane were acquired from the heat flow vs. temperature curve (Fig. 6) obtained from the DSC equipment. The temperature range from 24 °C to 29 °C constitutes the melting phase of the n-octadecane during the charging cycle, while the temperature range from 27 °C to 23.5 °C constitutes the solidification phase of the n-octadecane during the discharging cycle. The melting point of n-octadecane was found to be 28.07 °C, which is similar to the value reported by the manufacturer (Table 1). The latent heat values recorded during the heating and cooling cycles were found to be 202.5 J/g and 200.2 J/g.

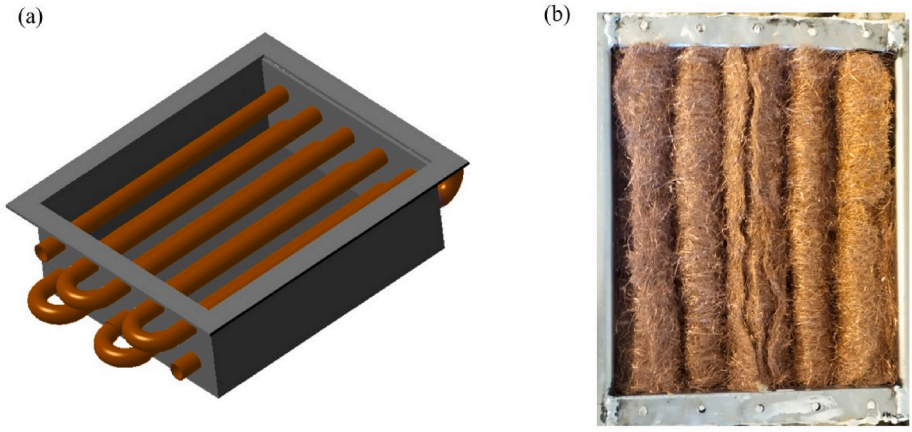

Fig. 5. TES tank (a) schematic representation of the TES tank without copper wool and (b) optical image of the TES tank with copper wool in design pattern 2.

Table 4
Operating conditions of the experimental setup.

Process	HTF inlet temperature (°C)	HTF flow rate (L/min)
Charging	45	3
Discharging	15	3

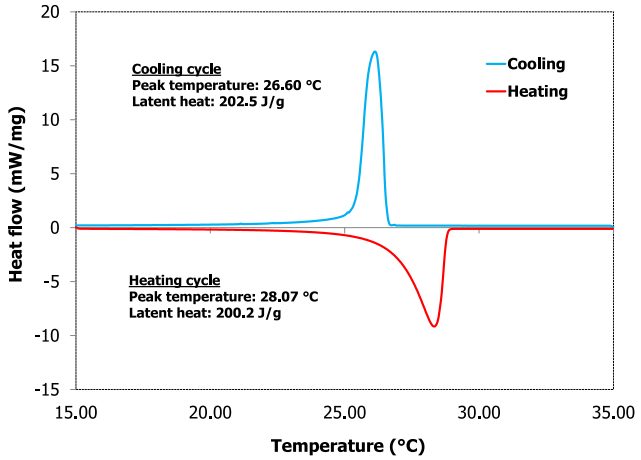

Fig. 6. Measured heat flow vs. temperature plot for n-octadecane.

3.2. Charging and discharging cycles

Figure 7 and 8 show the PCM temperature as a function of time during the charging and discharging cycles for the five configurations tested. The temperature range (15 °C–45 °C) covers both the latent and sensible heat components of the n-octadecane.

The TES tank containing only PCM (Baseline) exhibited a low charging rate (0.26 W) during the pre-melting phase. A nearly uniform temperature change rate (~0.21–0.31 W) was observed for the case 1 and case 3 configurations (copper wool in design pattern 1). However, the charging ramp was higher for the case 2 (0.52 W) and case 4 (0.42 W) configurations (copper wool in design pattern 2). Their latent and sensible heat components were also easily distinguishable from their charging curves.

The case 4 configuration emulated the ideal phase transition process (storing heat at a constant temperature) of an PCM. To the authors knowledge, this kind of behaviour was not found to be reported elsewhere in an experimental study employing PCM as an energy storage medium in TES system. The addition of copper wool with a high packing factor to the TES tank may facilitate PCM to store thermal energy at a constant temperature throughout the phase transition process.

Regarding the discharging cycle, the rates of discharge (0.38 W–0.57 W) were similar for all the tested cases during the early stage (45–30 °C) of the cycles. Since there was a significantly larger temperature difference between the HTF and the liquid PCM, the initial rate of discharge was the almost same for all cases. However, the case with only PCM (Baseline) exhibited a low rate of discharge (0.04 W) after the onset of the solidification process. The temperature change rate was higher for all the other cases, and they accomplished the following order in terms of the discharging rate: case 4 (0.15 W) > case 2 (0.09 W) > case 1 (0.07 W) > case 3 (0.06 W) > Baseline (0.04 W). As Figure 7 and 8 show, the addition of high-thermal-conductivity fillers to the TES tank results in a positive impact on both the charging and discharging rates.

3.3. Power and time comparison

Figure 9 and 10 depict the mean power (i.e., heat transfer rate) in the case of the distinct TES tank configurations and the corresponding time required for charging and discharging the PCM.

Here, the reported PCM melting time is the time required for the temperature of the n-octadecane to rise from 15 ± 1 °C to 29 ± 1 °C. In contrast, the solidification time is the time required for the temperature of the n-octadecane to drop from 45 ± 1 °C to 23.5 ± 1 °C. The selection of this particular temperature window was based on the end set temperatures of melting and solidification acquired from the heat flow curves of the n-octadecane.

During the charging cycle, the Baseline configuration (only PCM) took 0.45 h to transition from the solid phase to the liquid phase (15 °C–29 °C). However, the Case 3 configuration (coarse copper wool in design pattern 1) logged the lowest time (0.38 h) to undergo phase transition, with a 16 % reduction in time. In terms of the time required for melting the PCM, the different configurations can be ordered as follows: Case 3 < Case 2 < Case 4 < Case 1 < Baseline.

The mean power in all configurations was estimated using Eq. (1) for the charging cycle. Accordingly, the case 3 configuration (coarse copper wool in design pattern 1) attained a maximum value of the mean power of 381 W; a 53 % enhancement was observed compared to the Baseline configuration (only PCM).

The addition of high-thermal-conductivity copper wool positively impacts the mean power attained by the TES tank configurations. In the case 4 configuration (PCM and coarse copper wool in design pattern 2), despite of its high packaging factor, the reduction in the melting time was not appreciable. Therefore, adding copper wool is not the only factor responsible for the decrease in time required for melting. The two significant factors that come into play in enhancing heat transfer rate are the increased heat transfer surface area and the natural convection effects. The time required for melting the PCM gets drastically reduced

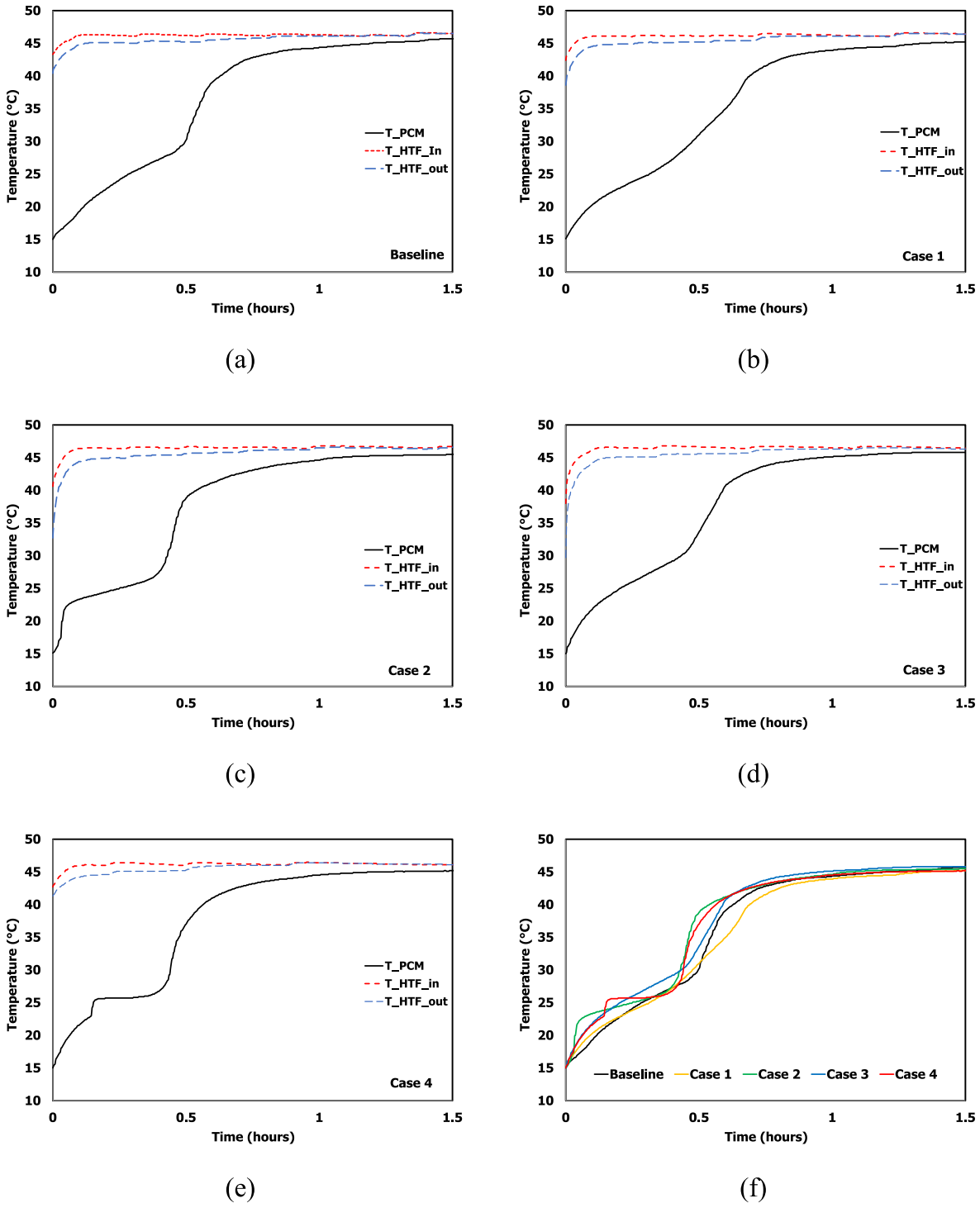

Fig. 7. Temperature vs. time plot during the charging cycle. (a) Baseline - only PCM, (b) Case 1 - PCM and fine copper wool in design pattern 1, (c) Case 2 - PCM and fine copper wool in design pattern 2, (d) Case 3 - PCM and coarse copper wool in design pattern 1, (e) Case 4 - PCM and coarse copper wool in design pattern 2 and (f) T_PCM comparison between TES tanks (see also Fig. 4).

when natural convection occurs. Zhang et al. [35] numerically investigated the melting performance of n-octadecane with and without natural convection effects. A reduction of 32.6 % in the time required for melting the PCM due to natural convection effects was reported. During the melting process of the PCM, the difference in the density of solid and liquid parts of the PCM promotes a natural convection effect [18,33,34]. Among all the developed design cases, the case 3 configuration (coarse copper wool), being the best performing among the three, seems to increase thermal conduction and, at the same time, leave enough space to promote the natural convection effects within the TES tank domain.

During the discharging cycle, the Baseline configuration (only PCM) took 2.9 h to transition from the liquid phase to the solid phase (45 °C–23.5 °C). The Case 4 TE S tank configuration (coarse copper wool in design pattern 2) logged the lowest time (43 min) to undergo phase transition with a 397 % reduction in time. The TES tank configurations can be ordered based on the time required for discharging the PCM as follows: Case 4 < Case 2 < Case 3 < Case 1 < Baseline.

The mean power in all configurations was estimated using Eq. (2) for

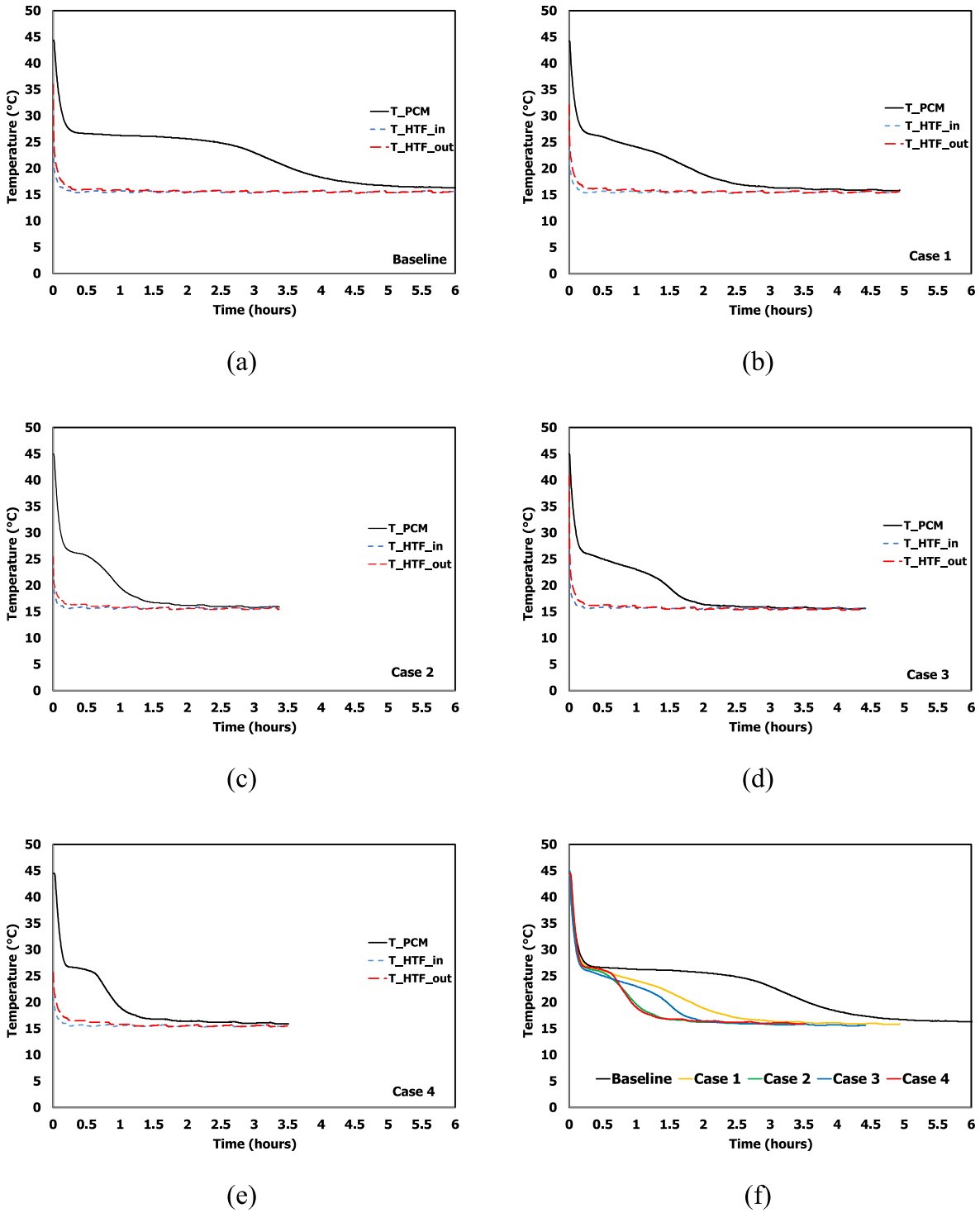

Fig. 8. Temperature vs time plot for the TES tank configurations during the discharging cycle. (a) Baseline - only PCM, (b) Case 1 - PCM and fine copper wool in design pattern 1, (c) Case 2 - PCM and fine copper wool in design pattern 2, (d) Case 3 - PCM and coarse copper wool in design pattern 1, (e) Case 4 - PCM and coarse copper wool in design pattern 2 and (f) T_PCM comparison between TES tanks.

the discharging cycle. Accordingly, the Case 4 configuration (coarse copper wool in design pattern 2) registered a maximum mean power of 213 W, i.e., a 205 % enhancement compared with the Baseline configuration. The TES tank configurations can be ordered based on the mean power for discharging the PCM as follows: Case 4 < Case 2 < Case 3 < Case 1 < Baseline. Heat conduction was the primary thermal transport mechanism that dominates the heat transfer rate during the solidification of the PCM. In this instance, the reduction in solidification time was in good agreement with the packaging factor of the copper wool in the different TES tank configurations. The higher the packaging factor (amount of metal wool), the more significant the time reduction for solidification. The TES tank configuration with the highest packaging factor has the lowest solidification time and the maximum value of the mean power. Thus, the addition of high-thermal-conductivity copper wool positively impacts the mean power of the TES tank also during the discharging cycle.

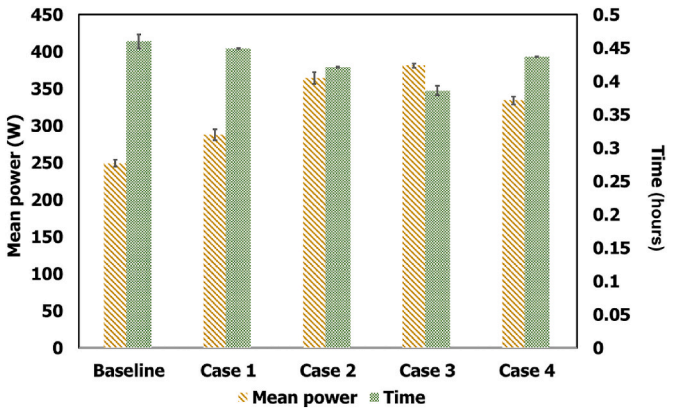

Fig. 9. Mean power vs. time comparison of the TES tank configurations during the charging cycle. Baseline - only PCM, Case 1 - PCM and fine copper wool in design pattern 1, Case 2 - PCM and fine copper wool in design pattern 2, Case 3 - PCM and coarse copper wool in design pattern 1, and Case 4 - PCM and coarse copper wool in design pattern 2.

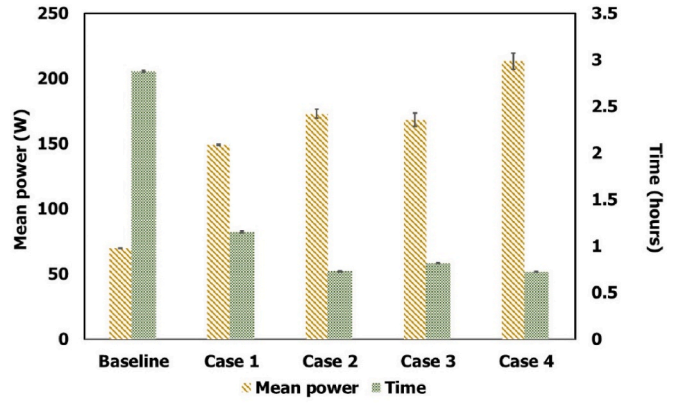

Fig. 10. Mean power vs. time comparison of the TES tank configurations during the discharging cycle. Baseline - only PCM, Case 1 - PCM and fine copper wool in design pattern 1, Case 2 - PCM and fine copper wool in design pattern 2, Case 3 - PCM and coarse copper wool in design pattern 1, and Case 4 - PCM and coarse copper wool in design pattern 2.

The total efficiency of the baseline TES tank was found to be 30 % using Equation (3). Of all the configurations developed, case 4 was found to have the highest efficiency (63 %). The following is the order of the configurations according to overall efficiency: case 4 > case 1 > case 2 > case 3 > baseline.

3.4. Total thermal energy storage capacity

The total energy stored in the TES tanks was estimated using the following expression:

$$TES = \sum_{T_{PCM=15\ ^\circ C}}^{T_{PCM=29\ ^\circ C}} \dot{m}_{HTF} C_p \left(T_{HTF,in} - T_{HTF,out}\right) \Delta t \tag{7}$$

The total energy stored by the TES tanks has been estimated for all the developed TES tank configurations. The results reveal that, when compared to other design configurations, the baseline configuration has the least amount of energy stored and the case 2 configuration has the highest amount of total energy stored. The energy stored in the Case 2 TES tank is 34 % more than that of the baseline configuration (412 kJ/kg). The increase in total energy storage for all configurations of TES tanks with metal wool was found to be primarily caused by the thermal resistance that developed between the metal wool's fibres and the phase change material. The metal wool's sensible heat component is the second mechanism that comes into the picture that enhances the TES tank's energy storage capacity. As a result, design configurations with the greatest number of fibres will have substantial energy storage capacities. Although the case 2 and case 4 configurations have the most fibres, the case 2 configuration has the finest fibres, therefore it will have more thermal resistance with the PCM and more total thermal energy storage.

4. Discussion and conclusions

The charging and discharging characteristics were obtained for the shell-and-tube-based TES tank configurations loaded with n-octadecane as PCM along the shell side and fed with water as the HTF along the tube side. Copper wool was chosen as a filler to improve the TES tank's effective heat transfer surface area, and two different wool thicknesses were tested in two different design patterns around the tubes of the TES tank. Accordingly, five shell-and-tube TES tank configurations were obtained, including the reference for performance evaluation. The performance of the TES tanks has been ascertained with a lab-scale experimental setup. Charging and discharging cycles were performed within the temperature window from 15 °C to 45 °C and 45 °C–15 °C, respectively. The measurements were repeated three times with the temperature data of the PCM and HTF recorded every 10 s.

In the case of melting, a decrease in the charging times has been obtained for all the configurations containing copper wools that have been tested. The TES tank configurations were ordered based on the time required for melting the PCM: case 3 < case 2 < case 4 < case 1 < Baseline. However, in the case of melting, the decrease in charging time is not proportional to the amount of wool added: in fact, the maximum amount of wool is present in the configuration of case 4, which is not the best performing configuration. This is due to the reduction in the natural convection by the presence of the highly packed copper wool. case 3 configuration registered the maximum value of the mean power (381 W) during the charging cycle; a 53 % enhancement was observed compared to the Baseline. This enhancement resulted in a decrease in the charging time of 16 %. And the total energy stored in the Case 2 TES tank is 34 % more than that of the baseline configuration (412 kJ/kg).

During the discharging process, the addition of the copper wool resulted in a decrease in the discharging times for all the configurations tested; the order in the discharging time is: case 4 < case 2 < case 3 < case 1 < Baseline. Being the solidification process mainly diffusive, the best-performing configuration during discharging (Case 4) generated a maximum value of the mean power of 213 W, a 205 % enhancement compared to the Baseline configuration. This enhancement resulted in a reduction in discharging time of 397 % compared to the Baseline. The addition of such high-thermal-conductivity metal wools positively impacted the charging and discharging rate. During the charging, the best enhancement was obtained when sufficient space for natural convection was present within the TES tank. On the other hand, being the solidification a purely diffusive process, the reduction in discharging time was linked with the amount of wool present within the TES tank.

It is noteworthy that the TES tank four design cases with metal wool integrated exhibited enhanced thermal performance. Thus, the copper wool proved to be a potential candidate to be chosen as the filler for a TES tank incorporating PCM. The incorporation of metal wools with high thermal conductivity had a beneficial effect on the thermal energy storage system charging and discharging rates. Notably, the inclusion of metal wool in the TES tank results in the PCM temperature remaining practically constant during the charging cycle, particularly when employing coarse copper wool with a higher packing factor (Case 4). The observed experimental behaviour closely approximates the ideal performance theoretically expected for PCM tanks. Lastly, despite the visual impression of a substantial amount of metal fibre, the actual quantity is relatively small and does not significantly diminish the storage capacity of the TES tank.

Working with metal wool revealed that it can be easily incorporated

into any system of interest to enhance its performance. Though we focused on a rectangular-shaped TES tank, their intrinsic adaptability allows them to be loaded in a TES tank of any shape. Being used in low-temperature TES systems in this investigation, there is literature demonstrating the suitability of metal wool for medium-temperature applications.

The results of this study suggest a list of design considerations that must be considered while constructing a TES tank that uses metal wool as an option to enhance effective thermal conductivity of the PCM.

1. Having a metal wool with two or three-dimensional heat transfer improves thermal transfer.
2. The thickness of the metal fibre significantly influences thermal performance, the thicker the metal fibre the better.
3. The metal wool packing factor and the discharging time were directly related.
4. The metal wool needs to be convoluted around the HTF tubes for improved charging rates, leaving enough room to encourage natural convection effects that enhances heat transfer.

CRediT authorship contribution statement

Alessandro Ribezzo: Writing – original draft, Validation, Methodology, Investigation, Formal analysis, Conceptualization. **Matteo Morciano:** Writing – review & editing, Formal analysis. **Gabriel Zsembinszki:** Writing – review & editing, Validation, Methodology, Investigation, Formal analysis, Conceptualization. **Sara Risco Amigó:** Writing – review & editing, Investigation. **Saranprabhu Mani Kala:** Writing – original draft, Visualization, Methodology, Investigation, Formal analysis, Conceptualization. **Emiliano Borri:** Writing – review & editing, Methodology, Investigation, Formal analysis, Conceptualization. **Luca Bergamasco:** Writing – review & editing, Methodology. **Matteo Fasano:** Writing – review & editing, Formal analysis. **Eliodoro Chiavazzo:** Writing – review & editing, Supervision, Resources, Project administration, Funding acquisition, Conceptualization. **Cristina Prieto:** Writing – review & editing, Project administration, Funding acquisition, Conceptualization. **Luisa F. Cabeza:** Writing – review & editing, Supervision, Resources, Project administration, Methodology, Investigation, Funding acquisition, Formal analysis, Data curation, Conceptualization.

Declaration of competing interest

The authors declare that they have no known competing financial interests or personal relationships that could have appeared to influence the work reported in this paper.

Acknowledgements

This project was funded by the European Union's Horizon Europe Research and Innovation Programme under grant agreement 101084182 (HYBRIDplus). Views and opinions expressed are however those of the author(s) only and do not necessarily reflect those of the European Union or CINEA. Neither the European Union nor the granting authority can be held responsible for them. This work was partially funded by the Ministerio de Ciencia e Innovación - Agencia Estatal de Investigación (AEI) (PID2021-123511OB-C31- MCIN/AEI/10.13039/501100011033/FEDER, UE and RED2022-134219-T). This work is partially supported by ICREA under the ICREA Academia programme. The authors would like to thank the Department de Recerca i Universitats of the Catalan Government for the quality accreditation given to their research group (2021 SGR 01615). GREiA is certified agent TECNIO in the category of technology developers from the Government of Catalonia.

References

[1] F. Perera, Pollution from fossil-fuel combustion is the leading environmental threat to global pediatric health and equity: solutions exist, Int. J. Environ. Res. Publ. Health 15 (2017) 16, https://doi.org/10.3390/ijerph15010016.
[2] M.M. Rahman, A.O. Oni, E. Gemechu, A. Kumar, Assessment of energy storage technologies: a review, Energy Convers. Manag. 223 (2020) 113295, https://doi.org/10.1016/j.enconman.2020.113295.
[3] A. Elkhatat, S.A. Al-Muhtaseb, Combined "renewable energy–thermal energy storage (RE–TES)" systems: a review, Energies 16 (2023) 4471, https://doi.org/10.3390/en16114471.
[4] R. Kothari, A. Ahmad, S. Kumar Chaurasia, O. Prakash, O. Prakash, Experimental analysis of the heat transfer rate of phase change material inside a horizontal cylindrical latent heat energy storage system, Mater Sci Energy Technol 5 (2022) 208–216, https://doi.org/10.1016/j.mset.2022.02.004.
[5] M. Imran Khan, F. Asfand, S.G. Al-Ghamdi, Progress in research and development of phase change materials for thermal energy storage in concentrated solar power, Appl. Therm. Eng. 219 (2023) 119546, https://doi.org/10.1016/j.applthermaleng.2022.119546.
[6] V.A. Lebedev, A.E. Amer, Limitations of using phase change materials for thermal energy storage, IOP Conf. Ser. Earth Environ. Sci. 378 (2019) 012044, https://doi.org/10.1088/1755-1315/378/1/012044.
[7] Z. Wang, J. Wu, D. Lei, H. Liu, J. Li, Z. Wu, Experimental study on latent thermal energy storage system with gradient porosity copper foam for mid-temperature solar energy application, Appl. Energy 261 (2020) 114472, https://doi.org/10.1016/j.apenergy.2019.114472.
[8] H. Koide, A. Kurniawan, T. Takahashi, T. Kawaguchi, H. Sakai, Y. Sato, J.N. W. Chiu, T. Nomura, Performance analysis of packed bed latent heat storage system for high-temperature thermal energy storage using pellets composed of micro-encapsulated phase change material, Energy 238 (2022) 121746, https://doi.org/10.1016/j.energy.2021.121746.
[9] S.S. Mundra, S.S. Pardeshi, Analysis of phase change material inside horizontally oriented heat storage unit: a numerical and experimental approach, Case Stud. Therm. Eng. 31 (2022) 101831, https://doi.org/10.1016/j.csite.2022.101831.
[10] P. Jidhesh, T.V. Arjunan, J. David Rathnaraj, Experimental investigation on heat transfer characteristics of phase change composite for thermal energy storage system, Mater. Today Proc. 42 (2021) 618–625, https://doi.org/10.1016/j.matpr.2020.10.949.
[11] A. Ribezzo, M. Fasano, L. Bergamasco, L. Mongibello, E. Chiavazzo, Multi-scale numerical modelling for predicting thermo-physical properties of phase-change nanocomposites for cooling energy storage, Tecnica Italiana-Italian Journal of Engineering Science 65 (2021), https://doi.org/10.18280/ti-ijes.652-409.
[12] A. Ribezzo, G. Falciani, L. Bergamasco, M. Fasano, E. Chiavazzo, An overview on the use of additives and preparation procedure in phase change materials for thermal energy storage with a focus on long term applications, J. Energy Storage 53 (2022), https://doi.org/10.1016/j.est.2022.105140.
[13] A.A. Al-Abidi, S. Mat, K. Sopian, M.Y. Sulaiman, A.Th. Mohammad, Internal and external fin heat transfer enhancement technique for latent heat thermal energy storage in triplex tube heat exchangers, Appl. Therm. Eng. 53 (2013) 147–156, https://doi.org/10.1016/j.applthermaleng.2013.01.011.
[14] A.A. Al-Abidi, S. Mat, K. Sopian, M.Y. Sulaiman, Abdulrahman.Th. Mohammad, Experimental study of melting and solidification of PCM in a triplex tube heat exchanger with fins, Energy Build. 68 (2014) 33–41, https://doi.org/10.1016/j.enbuild.2013.09.007.
[15] A. Gil, G. Peiró, E. Oró, L.F. Cabeza, Experimental analysis of the effective thermal conductivity enhancement of PCM using finned tubes in high temperature bulk tanks, Appl. Therm. Eng. 142 (2018) 736–744, https://doi.org/10.1016/j.applthermaleng.2018.07.029.
[16] A. Belazreg, A. Abderrahmane, N.A.A. Qasem, N. Sene, S. Mohammed, O. Younis, K. Guedri, N. Nasajpour-Esfahani, D. Toghraie, Effect of Y-shaped fins on the performance of shell-and-tube thermal energy storage unit, Case Stud. Therm. Eng. 40 (2022) 102485, https://doi.org/10.1016/j.csite.2022.102485.
[17] A. Surya, R. Prakash, N. Nallusamy, Heat transfer enhancement and performance study on latent heat thermal energy storage system using different configurations of spherical PCM balls, J. Energy Storage 72 (2023) 108643, https://doi.org/10.1016/j.est.2023.108643.
[18] Y. Xu, C. He, Y. Chen, Y. Sun, H. Yin, Z.-J. Zheng, Experimental and numerical study on the effect of the intelligent memory metal fin on the melting and solidification process of PCM, Renew. Energy 218 (2023) 119366, https://doi.org/10.1016/j.renene.2023.119366.
[19] N. Prasanth, M. Sharma, R.N. Yadav, P. Jain, Designing of latent heat thermal energy storage systems using metal porous structures for storing solar energy, J. Energy Storage 32 (2020) 101990, https://doi.org/10.1016/j.est.2020.101990.
[20] M. Morciano, M. Alberghini, M. Fasano, M. Almiento, F. Calignano, D. Manfredi, P. Asinari, E. Chiavazzo, 3D printed lattice metal structures for enhanced heat transfer in latent heat storage systems, J. Energy Storage 65 (2023) 107350, https://doi.org/10.1016/j.est.2023.107350.
[21] A. Favache, P. Bollen, X. Bollen, G. Baudoin, T. Pardoen, Metallic wool for enhanced thermal conductivity of phase change materials, Int. J. Therm. Sci. 193 (2023) 108468, https://doi.org/10.1016/j.ijthermalsci.2023.108468.
[22] C. Prieto, C. Rubio, L.F. Cabeza, New phase change material storage concept including metal wool as heat transfer enhancement method for solar heat use in industry, J. Energy Storage (2021) 101926, https://doi.org/10.1016/j.est.2020.101926.
[23] J. Gasia, J.M. Maldonado, F. Galati, M. De Simone, L.F. Cabeza, Experimental evaluation of the use of fins and metal wool as heat transfer enhancement

techniques in a latent heat thermal energy storage system, Energy Convers. Manag. 184 (2019) 530–538, https://doi.org/10.1016/j.enconman.2019.01.085.
[24] S.A. Marzouk, M.M. Abou Al-Sood, E.M.S. El-Said, M.M. Younes, M.K. El-Fakharany, Evaluating the effects of bifurcation angle on the performance of a novel heat exchanger based on contractual theory, Renew. Energy 219 (2023) 119463, https://doi.org/10.1016/j.renene.2023.119463.
[25] A.M. Abdulateef, J. Abdulateef, K. Sopian, S. Mat, A. Ibrahim, Optimal fin parameters used for enhancing the melting and solidification of phase-change material in a heat exchanger unite, Case Stud. Therm. Eng. 14 (2019) 100487, https://doi.org/10.1016/j.csite.2019.100487.
[26] D. Li, C. Yang, H. Yang, Experimental and numerical study of a tube-fin cool storage heat exchanger, Appl. Therm. Eng. 149 (2019) 712–722, https://doi.org/10.1016/j.applthermaleng.2018.12.024.
[27] S.A. Tat, P. Muthukumar, P.K. Mondal, Design, development and performance investigations of a latent heat storage with PCM encapsulation, J. Energy Storage 72 (2023) 108695, https://doi.org/10.1016/j.est.2023.108695.
[28] G.S. Sodhi, A.K. Jaiswal, K. Vigneshwaran, P. Muthukumar, Investigation of charging and discharging characteristics of a horizontal conical shell and tube latent thermal energy storage device, Energy Convers. Manag. 188 (2019) 381–397, https://doi.org/10.1016/j.enconman.2019.03.022.
[29] C. Nie, S. Deng, J. Liu, Effects of fins arrangement and parameters on the consecutive melting and solidification of PCM in a latent heat storage unit, J. Energy Storage 29 (2020) 101319, https://doi.org/10.1016/j.est.2020.101319.
[30] C. Prieto, C. Rubio, L.F. Cabeza, New phase change material storage concept including metal wool as heat transfer enhancement method for solar heat use in industry, J. Energy Storage (2021) 101926, https://doi.org/10.1016/j.est.2020.101926.
[31] S. Yu, X. Wang, D. Wu, Microencapsulation of n-octadecane phase change material with calcium carbonate shell for enhancement of thermal conductivity and serving durability: synthesis, microstructure, and performance evaluation, Appl. Energy 114 (2014) 632–643, https://doi.org/10.1016/j.apenergy.2013.10.029.
[32] H.A. Adine, H. El Qarnia, Numerical analysis of the thermal behaviour of a shell-and-tube heat storage unit using phase change materials, Appl. Math. Model. 33 (2009) 2132–2144, https://doi.org/10.1016/j.apm.2008.05.016.
[33] J.P. Holman, Experimental Methods for Engineers, eighth ed., McGraw-Hill, New York, 2012.
[34] S. Bell, A Beginner's Guide to Uncertainty of Measurement, second ed., National Physics laboratory, 1999.
[35] Y. Huang, C. Fan, B. Li, C. Zhang, Buoyancy-driven melting and solidification heat transfer in finned latent heat storage units, Int. J. Heat Mass Tran. 214 (2023) 124430, https://doi.org/10.1016/j.ijheatmasstransfer.2023.124430.